Basic evaluation of separator type specific phenomena of polymer electrolyte membrane fuel cell by the measurement of water condensation characteristics and current density distribution

Yutaka TABE[a, *], Kazushige KIKUTA[a], Takemi CHIKAHISA[a]

and Masaya KOZAKAI[b]

[a]Division of Energy and Environmental Systems, Graduate School of Engineering, Hokkaido University

N13 W8, Kita-ku, Sapporo 060-8628, Japan

[b]Department of Battery and Fuel Cell Systems, Hitachi Research Laboratory, Hitachi, Ltd., Japan

1-1, Omika-cho, 7-chome, Hitachi 319-1292, JAPAN

[*] Corresponding author. Tel.: +81 11 706 6381; fax: +81 11 706 7889.

E-mail address: tabe@eng.hokudai.ac.jp; N13 W8, Kita-ku, Sapporo 060-8628, Japan.

Abstract

This paper investigates phenomena related to water condensation behavior inside a polymer electrolyte membrane fuel cell (PEMFC), and analyzes the effects of liquid water and gas flow on the performance of the fuel cell. A method for simultaneous measurements of the local current density across the reaction area and direct observation of the phenomena in the cell are developed. Experimental results comparing separator types indicate the effect of shortcut flow in the gas diffusion layer (GDL) under the land areas of serpentine separators,

and also show the potential of straight channel separators to achieve a relatively-uniform current density distribution. To evaluate shortcut flows under the land areas of serpentine separators, a simple circuit model of the gas flow is presented. The analysis shows that slight variations in oxygen concentration caused by the shortcut flows under the land areas affect the local and overall current density distributions. It is also shown that the establishment of gas paths under the water in channels filled with condensed water is effective for stable operation at low flow rates of air in the straight channels.

Keywords: PEM fuel cell, Water condensation, Current density, Separator type, Gas diffusion layer, Shortcut flow

1. Introduction

Management of the water and gas flow is essential to realize uniform current densities across the reaction areas and to maintain high performance of polymer electrolyte membrane fuel cells (PEMFCs). The membrane needs to be fully hydrated to maintain high proton conductivity, but excess amounts of water condensed in the gas diffusion layers (GDLs) and gas flow channels impede the supply of reactants to the electrodes under high current density and low air flow rate conditions. Excess water causes mass transport limitations and deteriorates the cell performance, and the objective of this paper is to evaluate the effects of gas and liquid water flows inside PEMFCs.

Because experimental diagnostics, such as visualization of the water production behavior and measurement of the current density distribution, help develop a fundamental understanding PEMFC dynamics and provide benchmark-quality data for CFCD model validation, a number of studies on the diagnostics have been conducted, and an overview was provided on two-phase visualization, current distribution, high-frequency resistance distribution, mass distribution and temperature distribution [1]. The water production behavior in the cathode separator channel has been investigated using transparent fuel cells, and the relation between liquid water behavior and the cell performance was demonstrated [2,3]. Liquid water removal from gas channels has also been characterized in detail [4]. The effects of the distribution of the produced water and the gas composition on the cell performance were discussed using the measured results of the current density distribution [5,6]. For the relationships among the local phenomena, the distribution of pure ohmic cell resistance, the diffusivity of the electrodes and the free gas volume of the cell have been measured using the galvanostatic discharge of a fuel cell [7]. The simultaneous measurements of species concentration and current density distributions were conducted using a segmented cell [8], and the experimental approach using these distributions to measuring the spatially resolved water crossover coefficient was reported [9]. The authors here observed phenomena related to water production behavior inside a cell and analyzed the effects on the current and temperature distributions across the reaction area [10]. Other relationships between the local humidity and current distribution [11], and between the local cell impedance and current density [12] have also been investigated. However, to elucidate further details of the effect and mechanism of

local phenomena on the cell performance, wide ranging research with different experiments is necessary.

A fuel cell allowing direct observation of phenomena in the cell and measurements of the local current density and pressure drop distribution, with the help of windows in the cathode plate was developed, and the water production behavior on the surface of the GDL was observed through the open channels of the metal separator. The current density distribution was measured with insulated pins placed at 25 points in the anode separator, and measurements of the pressure drop distribution used an acrylic window with 15 holes along one channel of a serpentine separator.

The effect of the separator type on the cell performance was investigated using separators with straight and serpentine channels. The experimental results indicate a cell performance effect of shortcut flows in the GDL under the land areas (in the following termed lands) of serpentine separators. The results showed the potential of the straight channel separator to achieve a relatively-uniform current density distribution if the condensed water can be removed efficiently. The former, shortcut flows in a serpentine channel system, was also examined by 3-dimensional numerical simulation [13]; this study developed a simple circuit model of gas flow to evaluate shortcut flows under the lands of serpentine separators, and its validity was confirmed by measurements of the pressure drop distribution. Using this circuit model, the effect of shortcut flows in separator channels on the measured current density distribution was elucidated. Additionally, a unique phenomenon observed here [10] was investigated, suggesting a clue to methods for removing condensed water and supplying reactant gas efficiently to the membrane electrode assembly (MEA) in a straight channel cell.

In the flooded condition the cell voltage decreased gradually, followed by a sudden increase in voltage, and it was possible to operate the cell even when the cathode channel was filled with liquid water. The gas and liquid water behavior in the above phenomenon is discussed, and the effectiveness of applying the insight learned through this phenomenon was confirmed with stable air supply operation at low stoichiometric oxygen ratios.

2. Experimental apparatus and method

Experiments were conducted with two single cells, Cell I and Cell II, the two cells have similar structures each with an active area of 100 cm^2. The details of Cell I are in Reference [10]; Cell II includes improvements to Cell I realizing uniform clamping pressure across the reaction area, better cooling performance, and a larger observation area. An outline of the improved Cell II is shown in Fig. 1. A separator with straight channels was used on the anode side, and separators with straight or serpentine channels, as shown in Fig. 4 or 5, were used on the cathode side. The width of the channels and lands of both cathode separators were 2.0 mm. The cathode separators have open channels through which the GDL surfaces can be observed. The cathode separators were made of copper overlaid with gold, and the collected current was transmitted through the lands to the end metal-plates on both sides. The thickness of the separator, which corresponds to the channel height, was 0.5 mm, and the electric resistance in a plate with this structure was calculated to be adequately low. Further, 0.3 mm thick carbon papers were used for the GDLs; the cell was held together uniformly by 16 mm thick

end-plates at a clamping pressure of 1.2 MPa; and a 16 mm thick glass window was used for the direct observations.

The current density distribution was measured with 25 pins placed in the anode separator, the pin diameter was 5.5 mm, and the pins were electrically insulated as illustrated in Fig. 1 (bottom left). The surface of the separator was machined with the pins in place to create a flat surface of the assembly, and each pin was connected to a shunt resistance of 0.1 Ω for the current measurements. To compensate for contact resistance variations among the pins and to ensure uniform resistance over the whole area, calibration was made with a variable resistance connected to each shunt resistance as will be explained below. Additionally, a thin carbon cloth was placed over the GDL paper on the anode side to minimize variations in the contact resistance among pins.

In the experiments, the cell was set vertically as in Fig. 1, and placed in a thermostatic chamber. The cell temperature was kept constant by a water-cooled plate placed on the anode side without blocking the direct view. The experiments were conducted with pure hydrogen as the anode gas, and air (oxygen 21 %, nitrogen 79 %) or pure oxygen as the cathode gas. The outlet for the cathode gas was open to the chamber to avoid water plugging. The total pressure drop in the cathode gas flow was measured at the inlet connector of the cell, and the pressure drop distributions were measured with an acrylic window with 15 holes of 0.3 mm diameter along a single serpentine channel, as shown in Fig. 1 (bottom right). The cell resistance was measured by an alternating impedance meter at the impedance of 1 kHz, and the cell voltage, impedance, pressure drop, and current densities (actual voltage at the shunt resistance) were recorded on a computer at 4 second intervals.

At the start of the experiments, the overall cell resistance was set to a constant value by purging with dry nitrogen, and the variable resistance was adjusted to obtain a uniform current density distribution of 0.05 A cm^{-2} at a sufficient gas flow rate condition, where the current density was assumed to be uniform without an excess water production effect. Then, the overall cell resistance was set to the constant value by again purging with dry gases. With this procedure the initial condition provided good reproducibility in the current measurements. Experiments were started with various overall current densities, gas flow rates, and humidity conditions. Corrected current density distributions were used for the detailed analysis, here the current density differences between the average value for the 25 pins and the value at 0.05 A cm^{-2} were measured just after the start. The measured current differences at each point were then used to correct the measured current density as a ratio of the average current value during operation. This correction reduced measurement errors due to the slight resistance variations among pins which cannot be completely adjusted at low current densities.

3. Results and discussion

3.1. Liquid water behavior and current density distribution in straight and serpentine channels

The characteristics of the water production behavior, current density distribution, and cell performance in the straight and serpentine channel separators were investigated using Cell I. The overall current density was 0.4 A cm^{-2} and the flow rate of the cathode air was varied at

three different stoichiometric ratios. Pure hydrogen was supplied to the anode side at the stoichiometric ratio of 1.3. The humidity of both gases were set at the saturation temperature for 40 ℃, with the cell temperature at 50 ℃.

Figs. 2 and 3 show the cell voltage and pressure drop changes after the start of the power generation in the straight and serpentine separators. As the experiments progress, the pressure drops increase and the cell voltage decreases gradually in all experiments with both separators. The rate of the voltage drop is faster at the lower stoichiometric ratio, i.e. the smaller flow rate. At the lowest stoichiometric ratio, 1.4, the cell voltage drops significantly and operation could not be continued after around 2000 seconds with the straight separator, while the cell voltage was maintained at a stable level in the serpentine separator. These results confirm that the serpentine channel separator can be operated at the lower stoichiometric ratio.

Figs. 4 and 5 are direct views of the cathode channel and the current density distribution at two different times after the start of operation at the air stoichiometric ratio of 2.0 in the straight and serpentine separators. At this stoichiometric ratio, the cell voltage is similar for the two separators. After some time, liquid water droplets were observed in the channels in the downstream area, and the amount of condensed water in the serpentine channel was smaller than that in the straight channel as the drainage of liquid water from the serpentine channel is superior with the faster flow velocity of the gas. This better drainage makes it possible to operate at lower stoichiometric ratios with the serpentine channels.

Comparing the current density distributions (right half of Fig.4 and Fig.5), it is clear that the current density in the serpentine channel decreases on the down stream side (bottom in Fig. 5) at 300 seconds when little condensed water has appeared, and the current density

distribution increases at 2900 seconds. Despite less condensed water in the channel, the lack of uniformity in the current density distribution is more pronounced than in the straight channel. This is estimated to be caused by a lack of uniformity in the gas flow in the serpentine channel. The pressure drop is high in the serpentine channel, and shortcuts for gas flow through the GDL below the separator lands may form. Such shortcut paths in the GDL give rise to areas where the gas supply is insufficient, inducing the larger current density variation, as will be discussed later. Thus, the serpentine channel has the characteristics that the current density distribution easily becomes large even if no condensed water has been generated in the channel. The straight channel results suggest a potential to achieve a relatively-uniform current density distribution if the condensed water can be removed efficiently.

3.2. Gas flow in GDL under the lands of the serpentine separator and its effect on the current density distribution

To evaluate shortcut flows through the GDL under the serpentine separator lands between the channels, a simple circuit model of the gas flow was developed. This model is composed of 24 areas of resistance to the gas-flow along the channel including the flow in the GDL, K_1 to K_{24}, and 16 areas of resistance to the gas-flow through the GDL under the land, K_{25} to K_{37}, as suggested in Fig. 6. The modeled channel is representative for a channel with an average property of 5 parallel channels of a serpentine separator, and with Q as the flow rate. The parameters used in the circuit model are summarized in Table 1. The resistance in a channel,

k_C, was calculated by the equation for a laminar tube flow with rectangular cross-section, and the resistance in a 4 mm wide GDL, k_G, was estimated from the measured gas-flow resistance through the GDL using Cell II without channels, where 4.0 mm is the average GDL width for both gas-flows through channels and under the lands. The effect of the bends in the channel on the gas-flow resistance was measured using Cell II without GDL, and the correction factor at a bend in the channel in Table 1 expresses the ratio of the equivalent to the actual distances of the channel. The resistance of the gas-flow through the channel with GDL, k_{CG}, was calculated from k_C and k_G by the parallel relationship, $1/k_{CG} = 1/k_C + 1/k_G$. The resistances of K_1 to K_{24} were determined by multiplying k_{CG} by the actual distances of the channel, where K_4, K_6, K_9, K_{11}, K_{14}, K_{16}, K_{19}, and K_{21} each included half of the effect of a bend. In the K_{25} to K_{37} calculations, the resistance, k_G, and the shortcut distance of 10 mm were used.

To validate the simple circuit model of the gas flow, measurements of the pressure drop distribution were conducted using separators with 0.5 mm and 0.3 mm deep channels using Cell II. Fig. 7 shows the experimental and simulated pressure drop changes along the channel with and without GDL. Here, the abscissa is the equivalent position along the channel from the inlet including the influence of the bends. The air flow rate is 1018 cc min^{-1} (corresponding to a stoichiometric ratio of 1.4 at 0.4 A cm^{-2}). The simulated results of the circuit model are in good agreement with the experimental values. The pressure drop with the GDL is decreased by the shortcut flow in the GDL and, the effect is larger with the shallower channel. It is confirmed that the model can estimate the reduction in the total pressure drop by the shortcut flow under the lands and the detailed appearance of the pressure drop curve. Fig. 8 shows the flow rate distributions in both channels with GDL, where the experimental value

was calculated from the measured pressure drop changes in the case with GDL in Fig. 7. The variations in flow rate through the channel are expressed by the circle diameters and the shortcut flow rates under the lands are expressed by the percentages of the inlet flow rate. This figure clearly shows that the flow rate through the channel decreases due to the shortcut flow at the center of the cell. The rate of the shortcut flow has a maximum value at each corner and decreases along the channel in the flow direction. This is due to the larger pressure difference between adjacent channels at corners.

The current density distributions were measured to investigate the effect of shortcut flows through GDL under the lands using Cell II. The overall current density was 0.4 A cm^{-2} and the flow rate of the cathode air was at a stoichiometric ratio of 1.4. The humidity of both gases were set at the saturation temperature for 40 ℃, with the cell temperature at 50 ℃. Experiments were performed with the usual clamping pressure (1.2 MPa) reduced to 0.6 MPa to compare the effects of the shortcut flow rates under the lands. The lower clamping pressure decreases the gas-flow resistance in the GDL, it increases the shortcut flow rates, and decreases the total pressure drop. The resistance in the GDL at the clamping pressure of 0.6 MPa in Table 1 was estimated from the measured total pressure drop.

Fig. 9 shows the measured current density distributions and the current density along the channel from the inlet 240 seconds after the start of the experiments. The current density distribution at the clamping pressure of 0.6 MPa has become higher than that with 1.2 MPa, and this is considered to be due to the higher rate of shortcut flows. The current density decreases almost linearly with slight fluctuations along the channel, the amplitude of the current density is larger at the 0.6 MPa clamping pressure with the larger fluctuations induced

by the shortcut flows, and the overall gradient is also steeper. The estimated oxygen concentration shows change similar to the current density, the oxygen concentration calculated from the flow rate distribution by the circuit model assumed the rate of oxygen consumption to be equivalent to the average power generation. Fig. 10 shows the variations in the measured current density and the estimated oxygen concentrations from the average rates of decrease in current density and oxygen concentration at the clamping pressure of 0.6 MPa. These variations are similar to those of the current density and the oxygen concentration decreases at the middle parts of the straight channel segments. It may be postulated that these slight variations in oxygen concentration affect the local and overall current density distributions. The analysis was conducted at the condition where the effect of condensed water is negligible because it is difficult to estimate the gas-flow resistance under flooded conditions. Generally, the flooding increases the gas-flow resistance through channels, and the effect of shortcut flows on the cell performance can be anticipated to increase under flooded conditions.

3.3. Gas flow under channels filled with condensed water in the straight channels

The experimental results in the previous section compared separator types and indicated the possibility that straight channel cells can be operated with a relatively-uniform current density distribution, if the condensed water is removed efficiently. A unique phenomenon reported by the authors [10] was investigated as a method to remove condensed water and to supply reactant gas efficiently to the MEA.

Fig. 11 shows the cell voltage and pressure drop changes after the start of the power generation in the straight separator with oxygen as the cathode gas, and using Cell I. The overall current density was 0.4 A cm^{-2}. Pure hydrogen was supplied at the stoichiometric ratio of 1.3 and the oxygen at ratios of 2.5, 3.3, and 5.0. The humidity of both gases were set at the saturation temperature for 40 ℃ with the cell temperature itself at 50 ℃. These conditions easily cause flooding because the flow rate of the cathode oxygen is about one-fifth that of a cathode air flow at the same stoichiometric ratio. Fig. 12 is a direct view of the cathode channel and the current density distribution at two different times after the start of operation at the oxygen stoichiometric ratio of 2.5. The current densities were detected by the 25 pins without correction using the initial current distribution at 0.05 A cm^{-1} and they became higher than the overall density value, but it is still possible to discuss the changes in the current density distribution.

At 1100 seconds in Fig. 12, the channel paths are filled with liquid water from the downstream (right-hand) side and there is only a small region with the gas phase (white area enclosed with a dashed line). The other parts are filled by liquid water which appears as dark in the picture. During the operation the cell voltage at the oxygen stoichiometric ratio of 2.5 gradually decreases as in Fig. 11 and the current density distribution becomes larger, the cell appearing as in Fig. 12. After 1100 seconds, the gas phase pushes out the liquid water and the region filled with gas expands from the left. With this change, the area with high current density increases around the gas phase region, and the cell voltage increases abruptly as shown in Fig. 11. At 1700 seconds, the current distribution becomes uniform even though the region of the channel filled with condensed water remains, as shown in Fig. 12, and similar

phenomena were also observed at the other stoichiometric ratios. The cell voltage-drop starts earlier at the smaller ratios, the smaller flow rates, then the pressure drop increases after the cell voltage recovers, as a part of the liquid water is pushed out from the channels. The cell voltage stabilizes at a relatively high level, when the pressure drop becomes high, and the pressure variation also becomes larger at this stage. The final voltage, after the recovery, is higher for the smaller gas flow rates.

From the water behavior in the cathode channel, the changes in the cell voltage, and the pressure drop, the phenomena inside the GDL were hypothesized to be as illustrated in Fig. 13. In the early stage of operation (I), the produced water flows out to the channel though the relatively wide paths in the GDL, and accumulates at the surface of the GDL. Because of the hydrophilic properties of the glass window and metal separator, liquid water also spreads on the window and the separator surface. The volume of condensed water at the surface and maybe inside the GDL gradually increases, and the cell voltage drops correspondingly. At this stage there is still adequate space in the channel to allow gas flow and maintain an almost even pressure drop (phase I in the figure). Then a slight increase in the pressure drop pushes the liquid water in the channel to form water films along the window, and the liquid water is pulled from the surface and the inside of the GDL to the films, establishing gas paths under the liquid water on the window (phase II). This situation is further reinforced with a number of gas paths to the reaction area of the MEA, resulting in a stabilized satisfactory performance with a large pressure drop. Overall, this results in the sudden increase in the cell voltage (Fig, 11). Additionally, the effect where liquid water on the window attracts water from the GDL may play an important role in improving and stabilizing the cell performance. When the gas

flow rate is very high, no liquid water can accumulate in the channel, and only thin liquid water layers form along the window. This results in a lower pressure drop with the higher stoichiometric ratios, and the state becomes similar to phase I in Fig. 13, and would explain the cell voltage difference in Fig. 11. The above hypothesis for the process of the phenomena explains the changes in the cell voltage as well as the pressure drops well. Here, it must be noted that the process of the establishment of the gas-paths under the channels filled with condensed water is considered to be caused by the hydrophilic properties of the separator and the hydrophobic properties of the GDL.

This hypothesis suggests that the formation of a liquid layer in the vicinity of the channel surface is advantageous at flooded conditions, and such considerations were applied to realize stable air operation with low stoichiometric ratios. A condition where it is not possible to maintain operation with air was set with Cell I with a straight separator, the overall current density was 0.1 A cm^{-2} and the air flow rate of the cathode gas was at a stoichiometric ratio of 2.5; pure hydrogen was supplied to the anode side at the stoichiometric ratio of 1.3. The humidity of both gases were set at the saturation temperature for 40 ℃, with the cell temperature at 50 ℃. Fig. 14 shows the cell voltage and pressure drop changes for the case with first O_2 then air operation. To establish gas paths under the channels filled with condensed water, the operation with oxygen as the cathode gas took place at the same flow rate as with air, before the air operation. The overall current density was 0.5 A cm^{-2} and the oxygen flow rate of the cathode gas was at a stoichiometric ratio of 2.5. Similar phenomena as in the previous oxygen operation were observed before about 2300 seconds. Then the overall current density decreased to 0.1 A cm^{-2} and the cathode gas was changed to air at the

stoichiometric ratio of 2.5, which gives the same flow rate as with oxygen operation. This flow rate can maintain a channel filled with condensed water, and stable operation with air was continued for more than an hour, as shown in Fig. 14.

Fig. 15 summarizes the results of similar experiments for various overall current densities and stoichiometric ratios with air. A circle stands for where stable operation was achieved and a cross shows where stable operation was impossible, and triangles stand for cases where a determination was not possible. The solid marks including a cross are results where air was supplied from the start of the experiments, and the open circles for first O_2 then changed to air in manner in Fig. 14. Stable operation with only air as the cathode gas is difficult below a stoichiometric ratio of 5 because of flooding. However, operation with first oxygen then air realizes stable operation at a stoichiometric ratio of 2. These results suggest that the establishment of gas paths under channels filled with condensed water is effective for operation with low flow rates of air. The hypothesized process, however, must be evaluated by further investigation.

4. Conclusions

Using a fuel cell allowing direct observation of the phenomena in the cell as well as measurements of the local current density on the anode side and the local pressure drop in the cathode channel, the relationships among the local phenomena in two types of separators were investigated. The major conclusions may be summarized as follows:

1. Compared with a straight channel, the serpentine channel has better drainage of condensed water and operation at lower stoichiometric ratios with cathode air supply is possible. However, the serpentine channel has the characteristic that the variation in the current density easily becomes large because of shortcut flows through the GDL under the land areas even if condensed water is not accumulated in the channel.

2. The straight channel has the potential to achieve a relatively-uniform current density distribution when the condensed water is removed efficiently. One method of removing condensed water and supplying reactant gas efficiently to the MEA is presented, as described in conclusion 5 below.

3. A simple circuit model of the gas flow was developed to evaluate shortcut flows through the GDL under the land areas of the serpentine channel separators, and the validity of the model was confirmed by measurements of the pressure drop distributions. The analyses showed that shortcut flows through the GDL under the land areas decreases the total pressure drop and the flow rate through the channel at the center of the cell.

4. The slight variations in the oxygen concentration caused by the shortcut flows under the land areas of the serpentine separators were shown to affect the local and overall current density distributions.

5. In the straight channel, the establishment of gas paths under channels filled with condensed water is hypothesized to explain the unique experimentally determined changes in the cell voltage, water coverage in the channels, and pressure drops in the gas flow. It was also confirmed that the formation of the paths under condensed water is effective to allow low flow rate operation with air.

Acknowledgment

The authors thank N. Nohara and D. Yoshida (graduate students of Hokkaido University) for assistance with the experimental studies and the analyses.

References

[1] C. Y. Wang, Chem. Rev. 104 (2004) 4727-4766.

[2] K. Tüber, D. Pócza, C. Hebling, J. Power Sources 124 (2003) 403-414.

[3] X. G. Yang, F. Y. Zhang, A. L. Lubawy, C. Y. Wang, Electrochem. Solid-State Letters 7 (11) (2004) A408-A411.

[4] F. Y. Zhang, X. G. Yang, C. Y. Wang, J. Electrochem. Soc. 153 (2) (2006) A225-A232.

[5] M. Noponen, J. Ihonen, A. Lundblad, G. Lindbergh, J. Appl. Electrochem. 34 (2004) 255-262.

[6] Z. Liu, Z. Mao, B. Wu, L. Wang, V. M. Schmidt, V. M., J. Power Sources 141 (2005) 205-210.

[7] J. Stumper, M. Löhr, S. Hamada, J. Power Sources 143 (2005) 150-157.

[8] X. G. Yang, N. Burke, C. Y. Wang, K. Tajiri, K. Shinohara, J. Electrochem. Soc. 152 (4) (2005) A759-766.

[9] G. Q. Lu, F. Q. Liu, C. Y. Wang, J. Power Sources 164 (2007) 134-140.

[10] T. Chikahisa, Y. Tabe, K. Kikuta, N. Nohara, H. Shinohara, H., Proceedings of the 4th International Conference on Fuel Cell Science, Engineering and Technology [1/1 (CD-ROM) 97016], 2006, pp. 1-6.

[11] H. Nishikawa, R. Kurihara, S. Sukemori, T. Sugawara, H. Kobayasi, S. Abe, T. Aoki, Y. Ogami, A. Marsunaga, J. Power Sources 155 (2006) 213-218.

[12] W. H.J. Hogarth, J. Steiner, J. B. Benziger, A. Hakenjos, J. Power Sources 164 (2007) 464-471.

[13] L. Sun, P. H. Oosthuizen, K. B. McAuley, Int. J. Thermal Sciences 45 (2006) 1021-1026.

Fig. 1. Experimental apparatus for visual observations, current, and pressure measurements.

Fig. 2. Cell voltage and pressure drops in the cathode flow for three different stoichiometric ratios with air, λ = 1.4, 2.0, and 3.3, in the straight channel cell.

Fig. 3. Cell voltage and pressure drops in the cathode flow for three different stoichiometric ratios with air, λ = 1.4, 2.0, and 2.5, in the serpentine channel cell.

Fig. 4. Direct view of the straight channel cathode (left) and current density distribution (right) at 300 s and 3000 s in the Fig. 2 experiment for the 2.0 stoichiometric ratio.

Fig. 5. Direct view of the serpentine channel cathode (left) and current density distribution (right) at 300 s and 2900 s in the Fig. 3 experiment for the 2.0 stoichiometric ratio.

Fig. 6. Circuit model of the gas flow in the serpentine separator channel cell.

Fig. 7. Simulated and experimental results of the pressure drops along the serpentine channel for two different channel heights, *h*.

Fig. 8. Variations in flow rate through channel, expressed by circle diameter, and shortcut flow rates through GDL under the lands, expressed as percent of the total flow rate. The condition corresponds to with the GDL in Fig. 7 for the two channel heights, *h*.

Fig. 9. Current density distributions at two different clamping pressures, 1.2 and 0.6 MPa, for the 1.4 stoichiometric ratio, 240 seconds after the start of experiments.

Fig. 10. Variations in the measured current density and the estimated oxygen concentration at the 0.6 MPa clamping pressure.

Fig. 11. Cell voltage and pressure drops in the cathode flow in the flooded condition for three different stoichiometric ratios of oxygen, λ = 2.5, 3.3, and 5.0, in the straight channel cell.

Fig. 12. Direct view (left) and current density distribution (right) in the cathode channel at two different times in the Fig. 11 experiment for the 2.5 stoichiometric ratio. Dotted lines enclose areas with gas phase.

Fig. 13. Experimentally suggested liquid water distribution and gas flow paths: (I) the early stage of the gradual voltage drop, and (II) the stabilized high-voltage stage with large pressure drops.

Fig. 14. Cell voltage and pressure drop in the cathode flow for the case with first O_2 then (around 2300 s) changed to air.

Fig. 15. Operation with air alone and with first O_2 changed to air.

Table 1 Parameters in the simple circuit model.

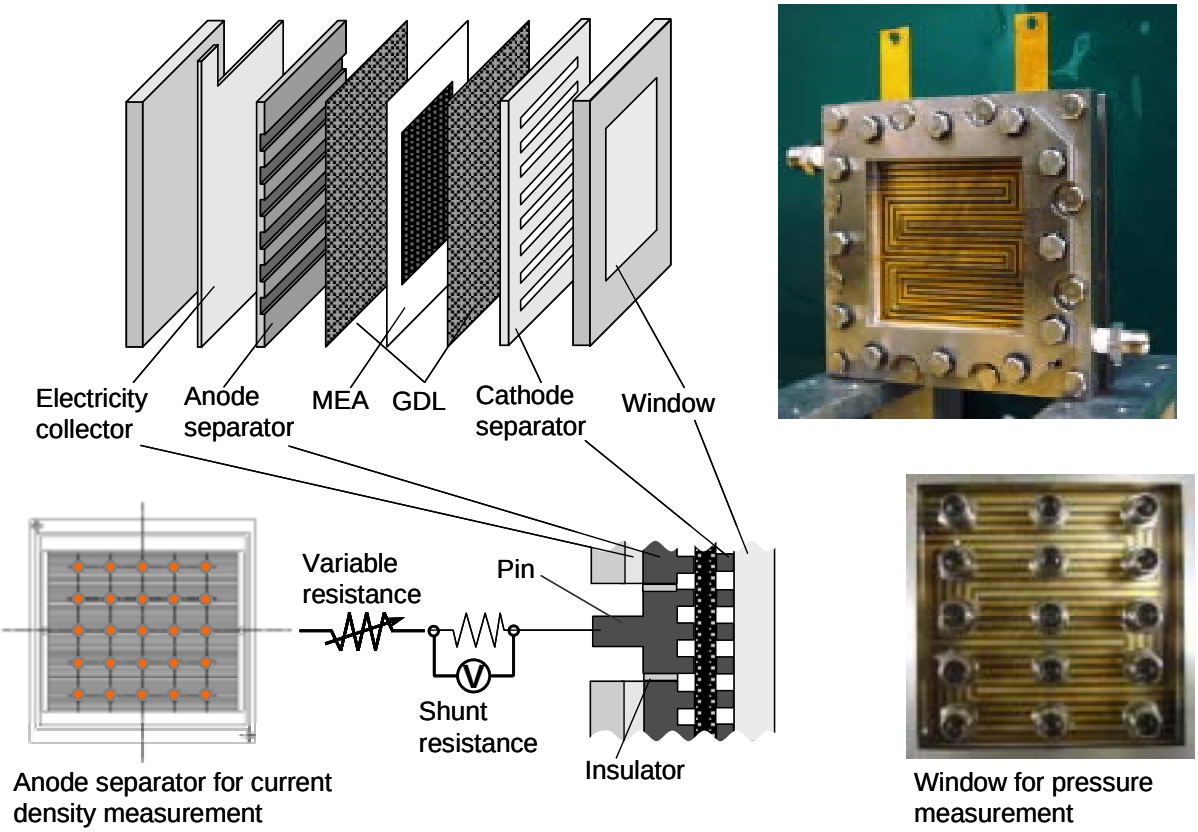
Electricity collector
Anode separator
MEA
GDL
Cathode separator
Window
Variable resistance
Pin
Shunt resistance
Insulator
Anode separator for current density measurement
Window for pressure measurement

Fig. 1

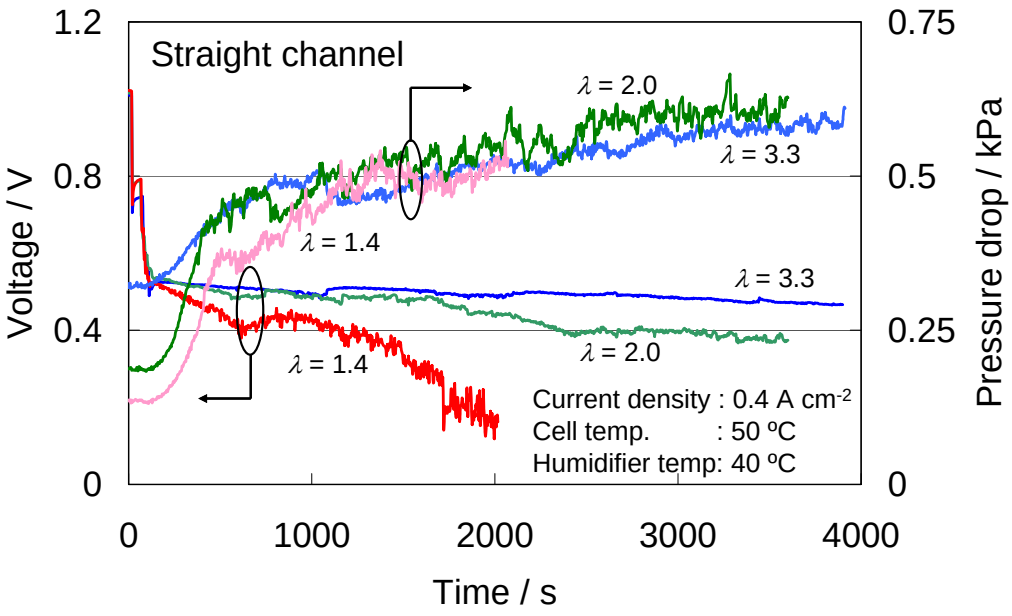

Fig. 2. Cell voltage and pressure drops in the cathode flow for three different stoichiometric ratios of air, λ = 1.4, 2.0 and 3.3, in the straight channel.

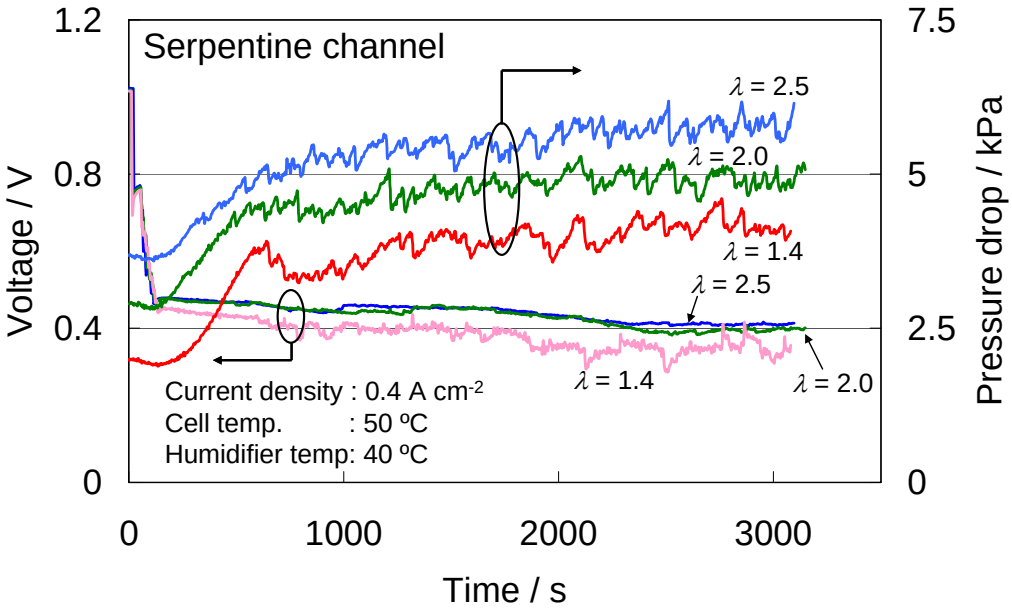

Fig. 3. Cell voltage and pressure drops in the cathode flow for three different stoichiometric ratios of air, λ = 1.4, 2.0 and 2.5, in the serpentine channel.

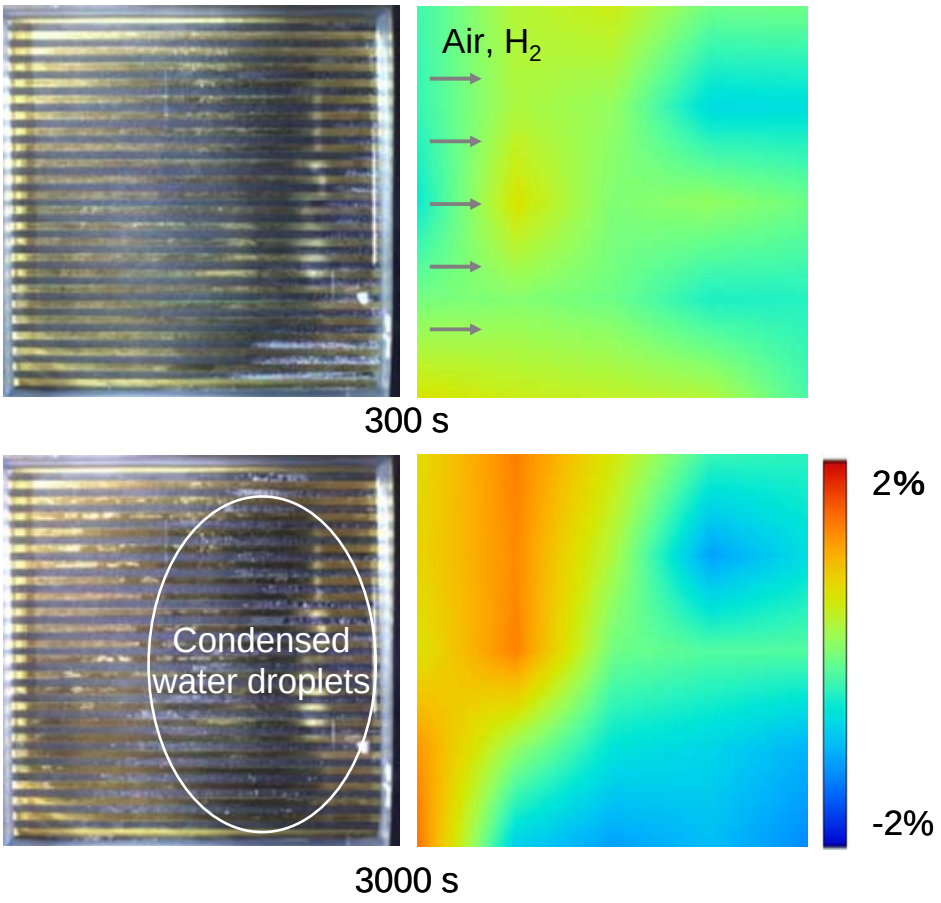

Fig. 4. Direct view in the cathode straight channel and current density distribution at two different times in the Fig. 2 experiment for the 2.0 stoichiometric ratio.

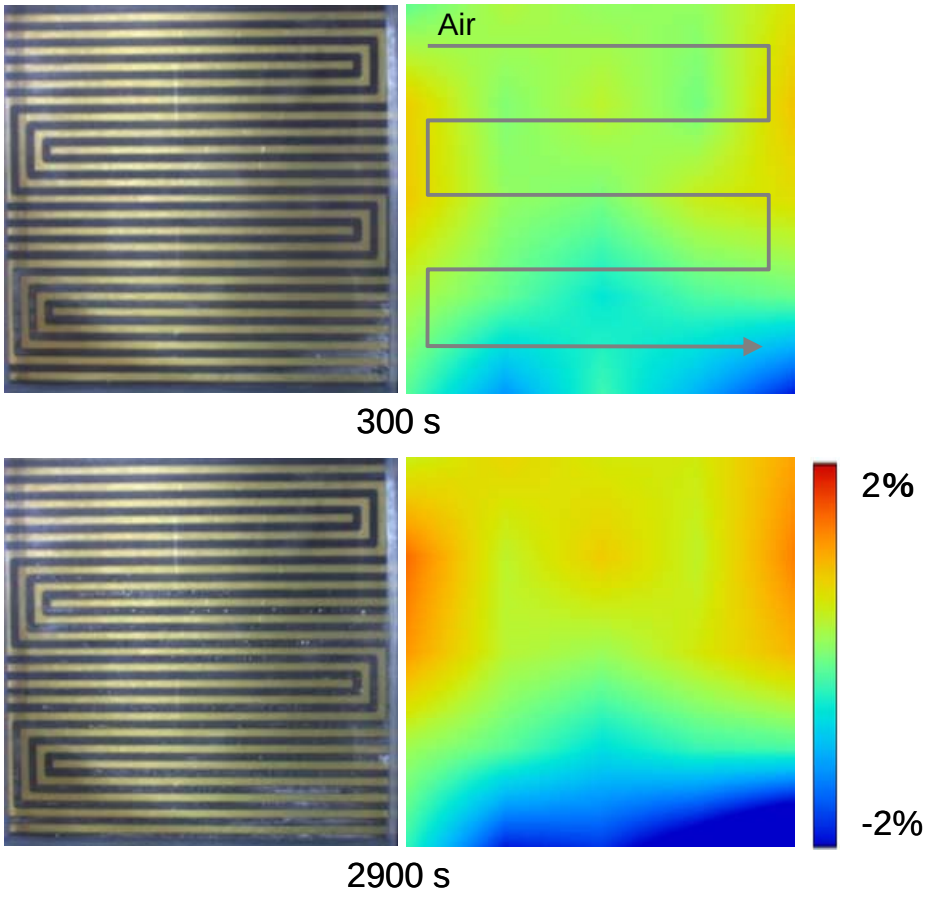

Fig. 5. Direct view in the cathode serpentine channel and current density distribution at two different times in the Fig. 3 experiment for the 2.0 stoichiometric ratio.

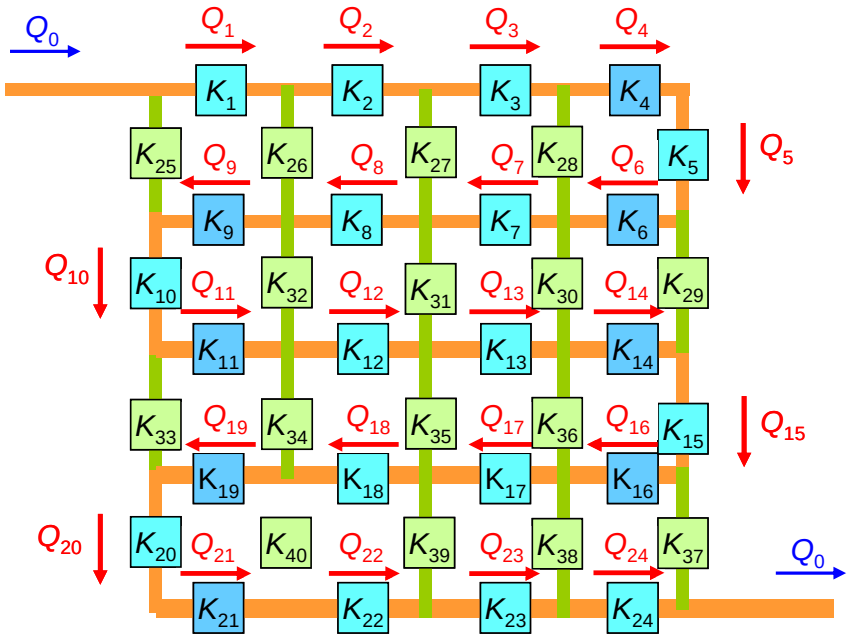

Fig. 6. Simple circuit model of the gas flow in the serpentine separator channel.

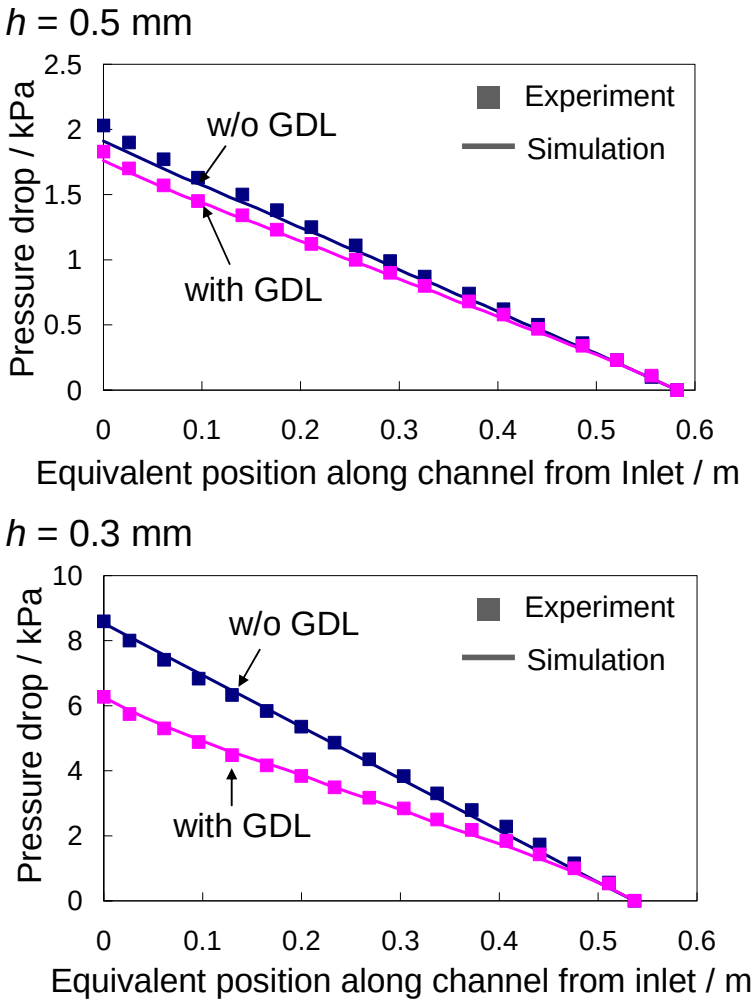

Fig. 7. Comparison between the simulated and experimental results of pressure drops along the serpentine channel for two different channel heights, *h*.

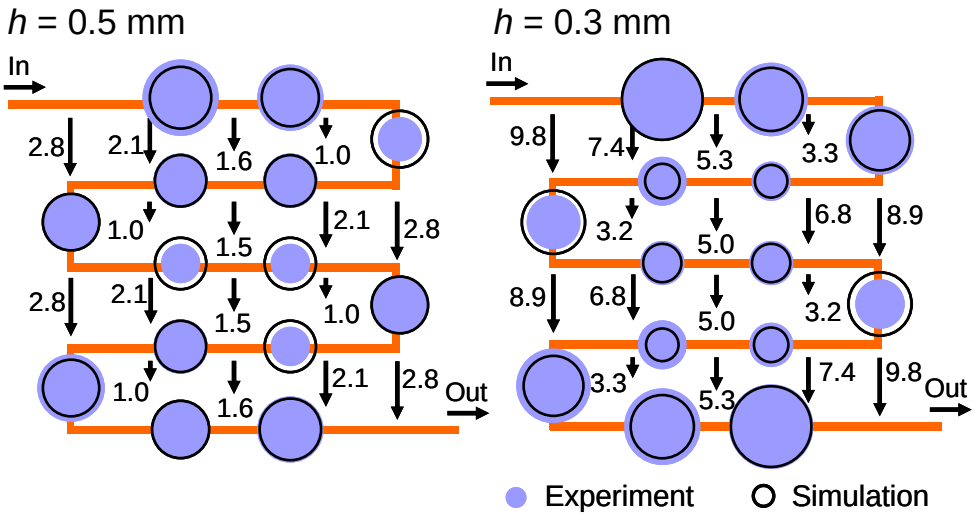

Fig. 8. Flow rate distributions through channel, expressed in circle size, and GDL under the lands, which is expressed in percentage of the total flow rate. The conditions correspond to the cases with GDL in Fig. 7 for two different channel heights, *h*.

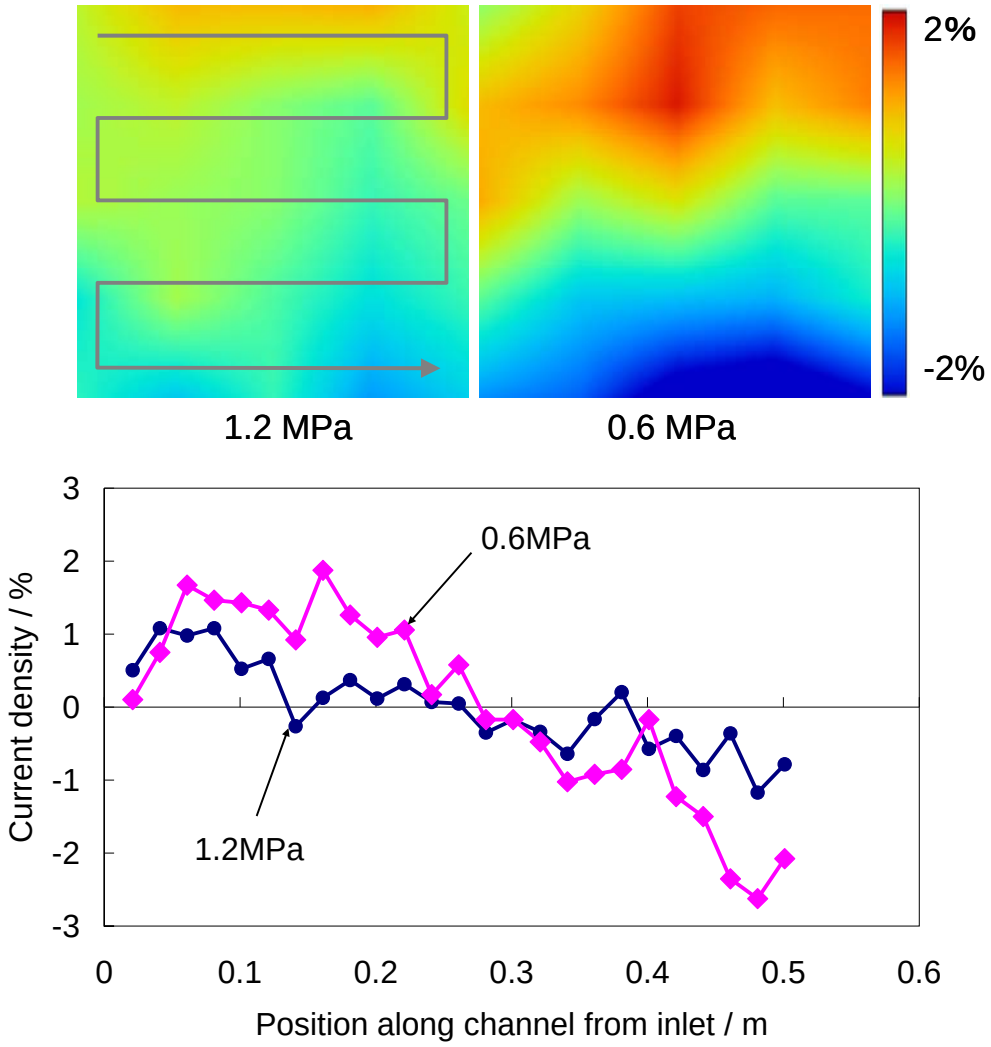

Fig. 9. Current density distributions at two different clamping pressures, 1.2 and 0.6 MPa, for the 1.4 stoichiometric ratio, 240 seconds after the start of experiments.

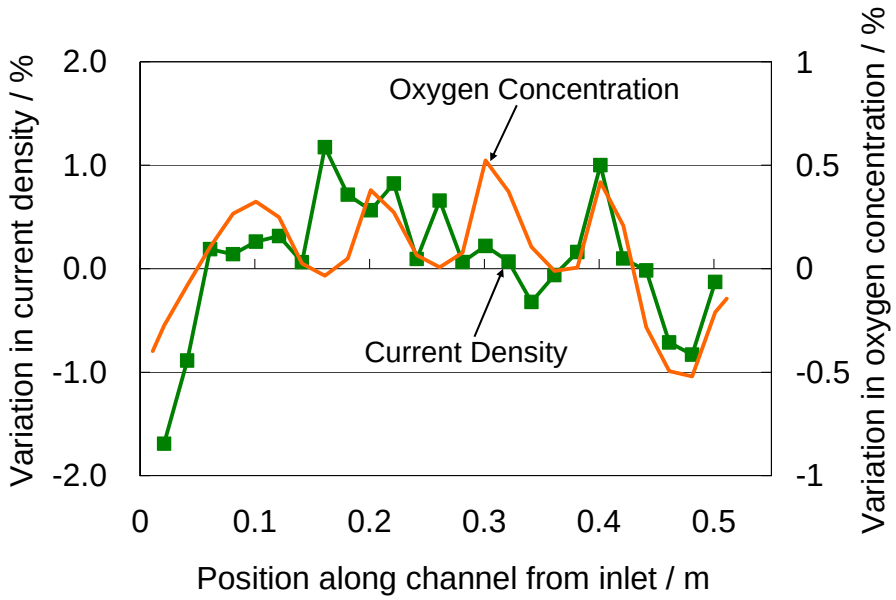

Fig. 10. Variations in the measured current density and the estimated oxygen concentration for the clamping pressure of 0.6 MPa.

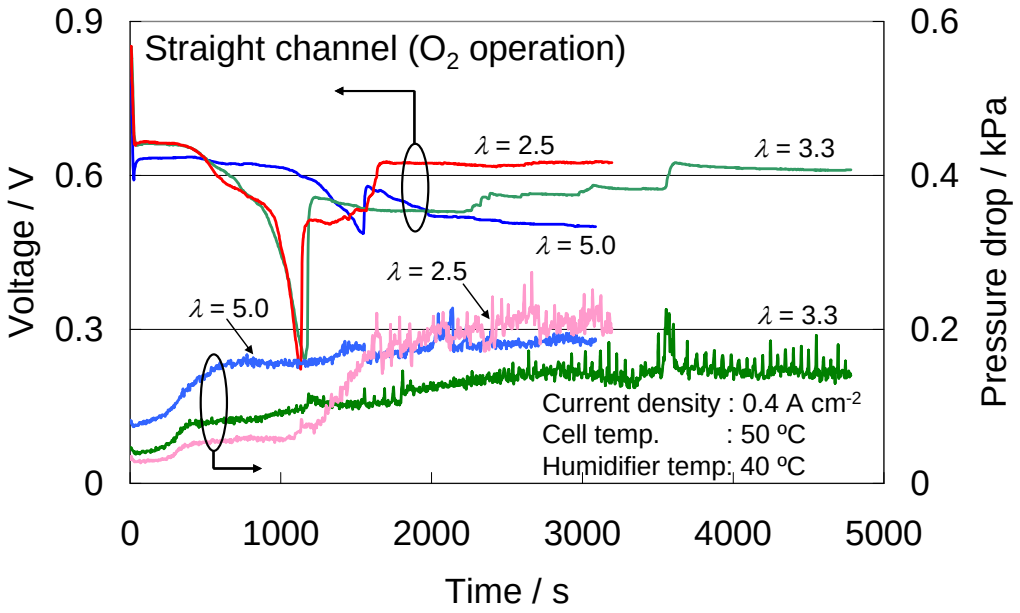

Fig. 11. Cell voltage and pressure drops in the cathode flow in the flooded conditions for three different stoichiometric ratios of oxygen, λ = 2.5, 3.3 and 5.0, in the straight channel.

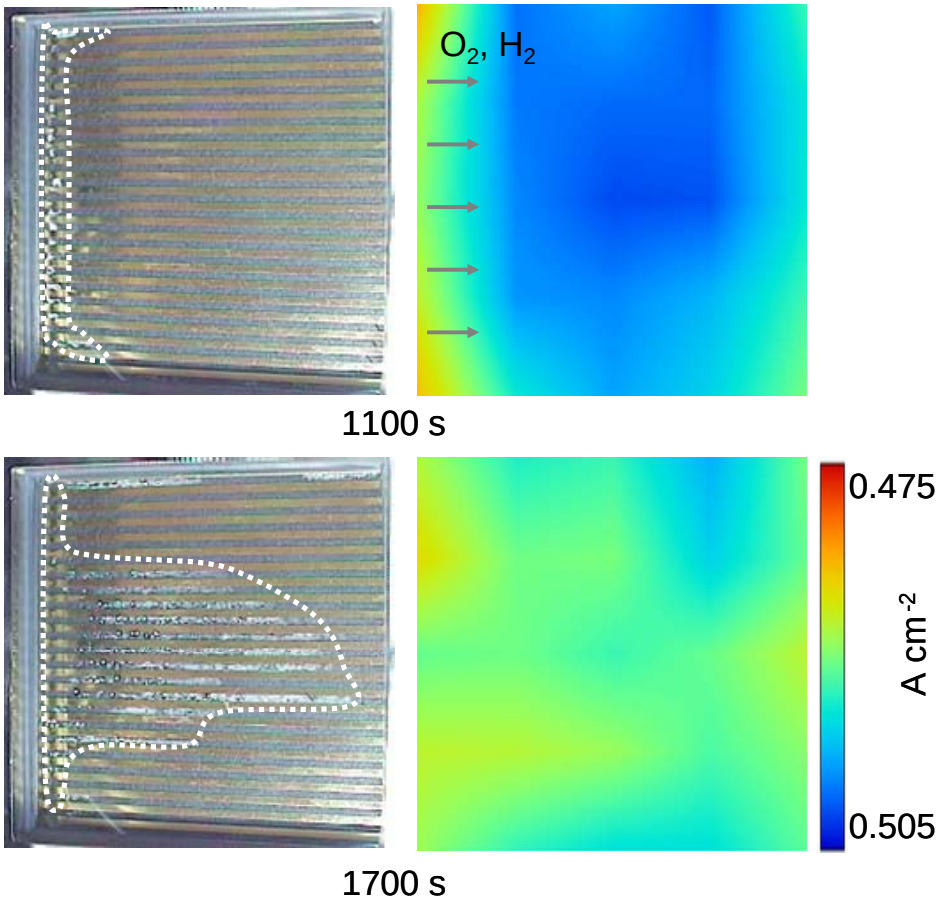

Fig. 12. Current density distribution and direct view in the cathode channel at three different times in the Fig. 11 experiment for the 2.5 stoichiometric ratio.

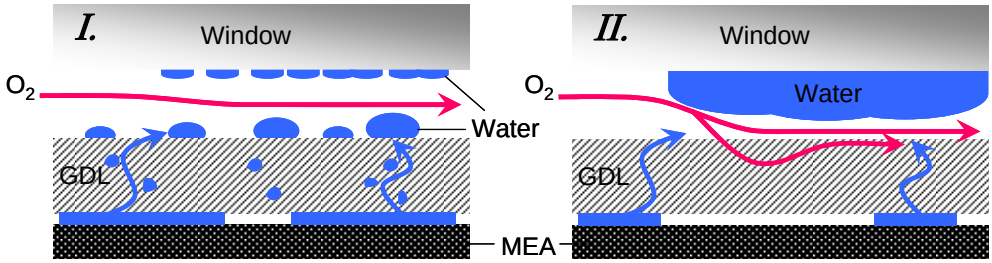

Fig. 13. Experimentally suggested liquid water distribution and gas flow paths: (I) corresponds to the early stage of the gradual voltage drop, and (II) for the stabilized high-voltage stage with large pressure drops.

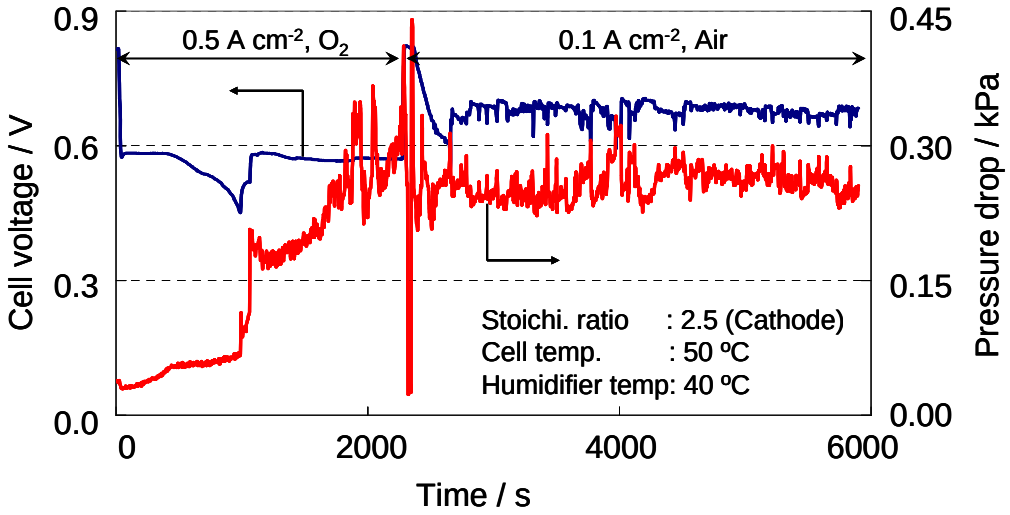

Fig. 14. Cell voltage and pressure drop in the cathode flow for the case with O_2-air exchanging.

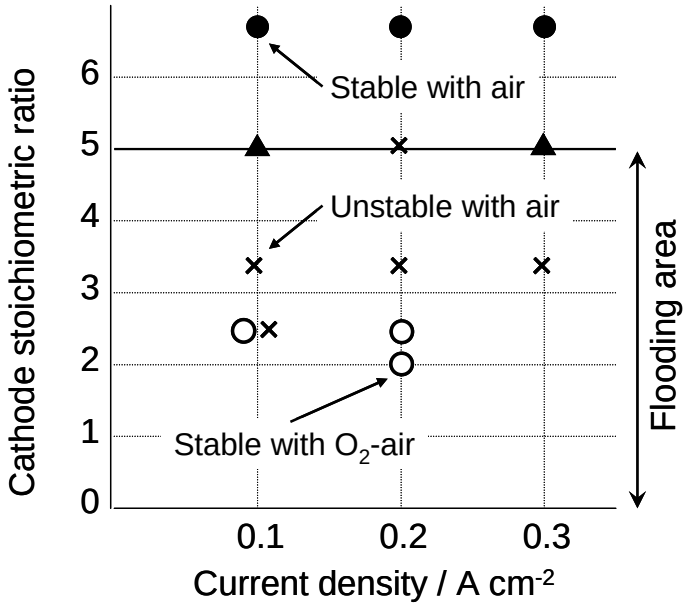

Fig. 15. Stability of operation with air and the case with O_2-air exchanging.

Table 1 Parameters in the simple circuit model.

Channel height [mm]	Flow resistance in channel [GPa s m^{-4}]	Corr. factor at bend [-]	Clamping press. [MPa]	Flow resistance in GDL [GPa s m^{-4}]
0.5	1.02	1.25	1.2	6.43×10^{2}
0.3	4.69	1.12	0.6	1.75×10^{2}